Geophysical characterization of hydrothermal systems and intrusive bodies, El Chichón volcano (Mexico)

Martin Jutzeler,[1,2] Nick Varley,[2] and Michael Roach[1]

Received 13 September 2010; revised 12 January 2011; accepted 21 January 2011; published 15 April 2011.

[1] The 1982 explosive eruptions of El Chichón volcano (Chiapas, Mexico) destroyed the inner dome and created a 1-km-wide and 180-m-deep crater within the somma crater. A shallow hydrothermal system was exposed to the surface of the new crater floor and is characterized by an acid crater lake, a geyser-like Cl-rich spring (soap pool), and numerous fumarole fields. Multiple geophysical surveys were performed to define the internal structure of the volcanic edifice and its hydrothermal system. We carried out a high-resolution ground-based geomagnetic survey in the 1982 crater and its surroundings and 38 very low frequency (VLF) transects around the crater lake. A 3-D inversion of the ground-based magnetic data set highlighted three high-susceptibility isosurfaces, interpreted as highly magnetized bodies beneath the 1982 crater floor. Inversion of a digitized regional aeromagnetic map highlighted four major deeply rooted cryptodomes, corresponding to major topographic highs and massive lava dome outcrops outside and on the somma rim. The intracrater magnetic bodies correspond closely to the active hydrothermal vents and their modeled maximum basal depth matches the elevation of the springs on the flanks of the volcano. Position, dip, and vertical extent of active and extinct hydrothermal vents identified by VLF-EM surveys match the magnetic data set. We interpret the shallow lake spring hydrothermal system to be mostly associated with buried remnants of the 550 BP dome, but the Cl-rich soap pool may be connected to a small intrusion emplaced at shallow depth during the 1982 eruption.

Citation: Jutzeler, M., N. Varley, and M. Roach (2011), Geophysical characterization of hydrothermal systems and intrusive bodies, El Chichón volcano (Mexico), *J. Geophys. Res.*, *116*, B04104, doi:10.1029/2010JB007992.

1. Introduction

1.1. Geophysical Surveys

[2] We conducted a variety of geophysical surveys in November 2006, March 2007, and October 2007 to investigate and quantify the subsurface structure of the volcanic edifice of El Chichón volcano (Chiapas, Mexico). Despite the remoteness of the volcano and the difficult environment, the floor of the 1982 crater remains relatively easy and safe to access. Our study focuses on two main research aspects: the hydrothermal system and the structure and geology of the volcanic complex. Hydrothermal activity is present in the 180-m-deep, 1-km-wide crater and is characterized by an acid lake, Cl-rich springs, and fumaroles. Three prominent structures to the E, NW, and SW of the recent crater were considered as old "domes" [*Layer et al.*, 2009; *Macías et al.*, 1997].

[3] The inner structure of a volcanic edifice is usually much more complex than the surficial expression [*Schmincke*, 2004]. To better understand the complexities related to the growth and destruction of El Chichón volcano, we carried out an extensive ground-based geomagnetic survey, the first of this kind on El Chichón, on the upper part of the edifice and in the 1982 crater and utilized a published aeromagnetic data set [*Servicio Geológico Mexicano*, 2006]. Inversion of those two data sets permitted us to characterize the morphology of the main underground magnetic bodies and to interpret them in comparison with previous studies [*Layer et al.*, 2009; *Macías et al.*, 1997, 2003; *Rose et al.*, 1984].

[4] One of the most challenging aspects related to understanding the hydrothermal system of El Chichón volcano has been the determination of the sources of the numerous flank springs associated with the volcanic edifice, and to trace the links between them and the surficial aquifers [*Rouwet et al.*, 2008, 2009; *Taran and Peiffer*, 2009; *Taran and Rouwet*, 2008; *Taran et al.*, 2008, 1998; *Tassi et al.*, 2009]. The shallow paths of the hydrothermal vents were characterized using very low frequency (VLF)-EM and ground-based geomagnetic techniques. These surveys are complementary to geochemical surveys carried out during the last decade [*Mazot and Taran*, 2009; *Rouwet et al.*, 2008, 2009; *Taran and Peiffer*, 2009; *Taran et al.*, 2008, 1998; *Tassi et al.*, 2009, 2003]. In this paper, we are following the nomenclature of *Layer et al.* [2009] for the volcanic units and *Taran and Peiffer* [2009] for the springs and other localities.

[1]Centre of Excellence in Ore Deposits, University of Tasmania, Hobart, Tasmania, Australia.
[2]Facultad de Ciencias, Universidad de Colima, Colima, Mexico.

0148-0227/11/2010JB007992

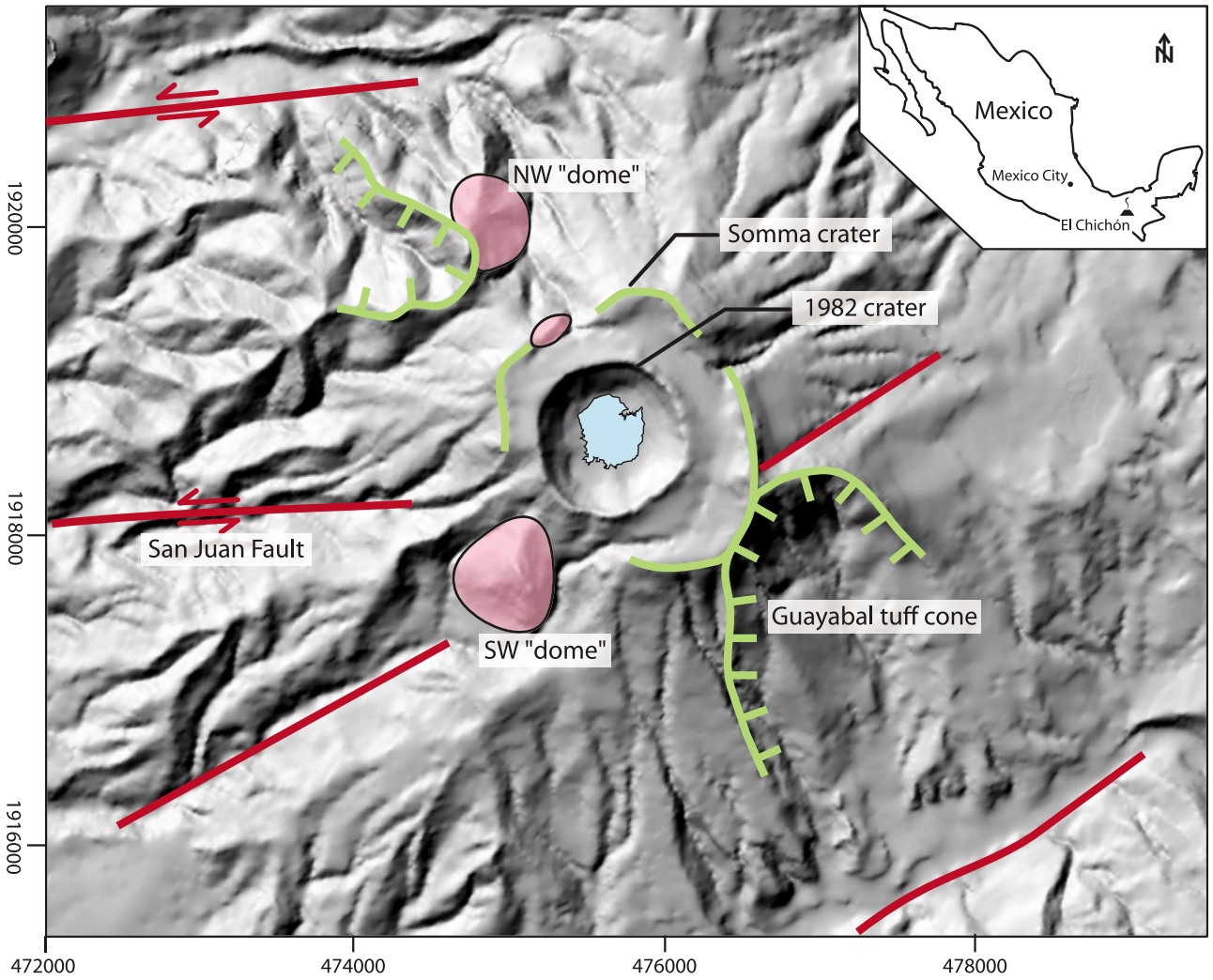

Figure 1. Shaded topographic map of El Chichón volcano. Blue line for crater lake (level of March 2007), red patches for major cryptodome outcrops, green lines for old craters and collapse scars, red lines for faults; coordinates in UTM. Modified after *García-Palomo et al.* [2004] and *Layer et al.* [2009].

1.2. Techniques

[5] The geomagnetic method, as applied here, involves recording total magnetic intensity (TMI) at the Earth's surface followed by forward modeling and inversion to the morphology and depth of buried magnetized bodies. Aeromagnetic surveys have been used to characterize intrusions and other nonporous volumes, alteration zones, and structural complexities of complete volcanic systems [*Araña et al.*, 2000; *Blanco-Montenegro et al.*, 2007; *Cassidy et al.*, 2007; *De Ritis et al.*, 2007; *Finn et al.*, 2001, 2007; *Hildenbrand et al.*, 1993; *Lénat and Aubert*, 1982; *Zlotnicki et al.*, 2009]. Ground-based surveys have only rarely been used to describe volcanic environments [*Hurst et al.*, 2004; *Napoli et al.*, 2007].

[6] The very low frequency (VLF)-EM method is an active source electromagnetic technique for rapidly mapping shallow subsurface conductivity variations. VLF instrumentation is highly portable because it utilizes distant very low frequency radio transmissions as an electromagnetic source. The VLF technique has been used in the search for ore deposits, for hydrology prospection, as well as in other domains of geophysics [*McNeill and Labson*, 1991; *Milsom*, 1996; *Monteiro Santos et al.*, 2006; *Sharma and Baranwal*, 2005]. Very few VLF studies have been performed in active volcanic areas. *Zablocki* [1978] and *Zlotnicki et al.* [2006] describe the application of VLF for mapping the extent and relative depth of fumarole sites, alteration zones, faults, shallow dykes, and partially melted lava bodies.

2. Geological Settings

2.1. El Chichón Volcano

[7] The most recent eruption of El Chichón volcano (17° 21.6′N–93°13.8′W, Chiapas, Mexico) occurred from 28 March to 4 April 1982 and formed a 1-km-wide, 180-m-deep crater within the wider (~2 km diameter) and higher (~1,100 m altitude) somma crater (Figure 1). The volcano is mainly trachy-andesitic in composition and constructed from a complex of "domes" and tuff cones; its apron is almost entirely constituted of volcaniclastic deposits composed of

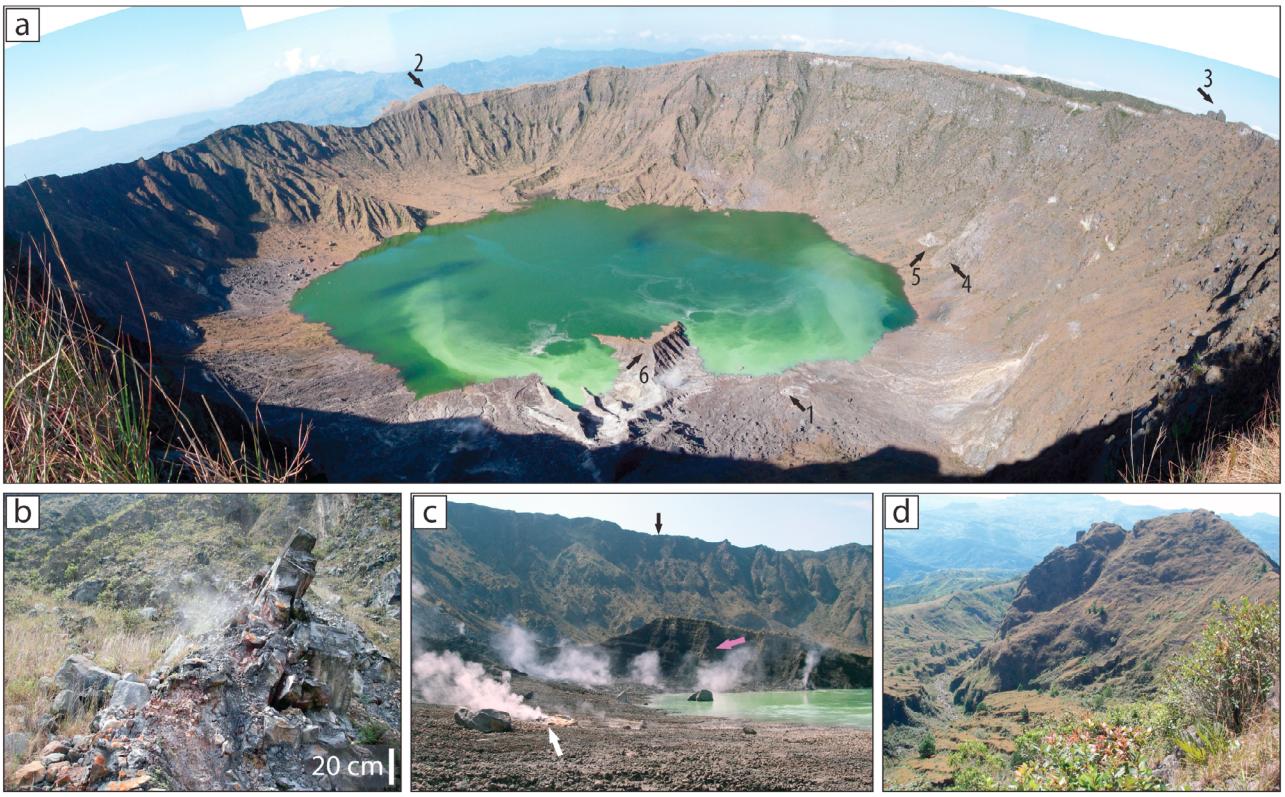

Figure 2. (a) The 1982 crater of El Chichón volcano (Chiapas, Mexico) viewed from the NNE. Light green colored waters in the crater lake (high level of March 2007) are associated with main hydrothermal activity. Soap pool (1), SW dome (2), small neck to the NW (3), old dome remnant (4), intracrater dyke (5), and mound of stratified postclimatic phreatomagmatic deposits (6). (b) Intracrater (1982?) dyke, still steaming. (c) Part of the active hydrothermal area on the NE side of the 1982 crater, soap pool (white arrow), mound of stratified post-climatic phreatomagmatic deposits (purple arrow), and 1982 crater rim with main trail to access the crater (black arrow) in the background. (d) SW cryptodome, >200 m high, with hot-spring-sourced river at its foot, view from the S rim of the 1982 crater.

products from block-and-ash flows and phreatomagmatic and Plinian eruptions [*Espíndola et al.*, 2000; *Layer et al.*, 2009; *Macías et al.*, 1997; *Rose et al.*, 1984]. The 1982 eruption was preceded by at least 11 eruptions during the last 8000 years which probably occurred mainly within the somma crater [*Espíndola et al.*, 2000].

[8] A centrally nested dome (1230 masl) was extruded within the somma crater after the Plinian eruption at 550 BP [*Espíndola et al.*, 2000; *Macías et al.*, 2003], and its basal talus breccia was separated from the somma crater by a ring depression called the "moat." During the 20th century, the dome was accompanied by intense fumarolic activity [*Canul et al.*, 1983; *Damon and Montesinos*, 1978; *Mulleried*, 1933]. The Plinian and phreatomagmatic eruptions of 1982 completely destroyed the dome, dispersing pyroclastic fallout at up to 72 km laterally from the vent with a maximum column height of 32 km [*Carey and Sigurdsson*, 1986; *Varekamp et al.*, 1984]. Pyroclastic flows traveled up to 5 km from the crater, with dilute surges to 8 km [*Scolamacchia et al.*, 2005]. Thickness of the pyroclastic flow deposits was 5–7 m on the flank of the volcano and reached >20 m in the moat area [*Macías et al.*, 1997], completely annihilating the "dense tropical forest" described by *Mulleried* [1933].

[9] Three peripheral "domes" are situated at the SE, NW, and SW of the somma crater (Figures 1 and 2) and were dated by Ar/Ar at 12 ka, 95 ka, and 217 ka, respectively [*Layer et al.*, 2009]. Field evidence shows they probably postdate the formation of the somma crater. The oldest rock of the edifice, an accidental lithic embedded in a pyroclastic flow deposit, was dated at 370 ka (Ar/Ar). The NW and SW "domes" have a very small aspect ratio with >200-m-high cliffs and a relatively small lateral extent (200–300 m). The SE dome is mostly buried by younger volcaniclastic deposits and outcrops on cliffs to the NNW of the Guayabal tuff cone (Figure 1; J. L. Macías, personal communication, 2010). The Guayabal tuff cone is situated to the SE of the somma crater and overlies dome rocks (J. L. Macías, personal communication, 2010). According to a regional gravity survey interpreted by *Medina et al.* [1990], the basement uniformly dips SW and residual positive anomalies were detected at the site of the three peripheral domes.

[10] The 1982 eruption had a catastrophic effect on the local population, with >2000 casualties and the destruction of local infrastructure [*Macías et al.*, 2008]; the release of an enormous amount of aerosols (especially SO_2) was recognized as resulting in worldwide climatic forcing [*Krueger*

et al., 2008; *Rampino and Self*, 1984]. Former eruptions likely had disastrous effects on ancient civilizations of Olmec or Maya origin [*Espíndola et al.*, 2000; *Nooren et al.*, 2009].

2.2. Hydrothermal System

[11] The hydrothermal system associated with the volcano comprises several springs outpouring acid to near-neutral, hot (up to 80°C) waters at the break-in-slope of the volcanic apron. These were already active before the 1982 eruption [*Casadevall et al.*, 1984; *Rouwet et al.*, 2008, 2009; *Taran and Peiffer*, 2009; *Taran et al.*, 2008, 1998; *Tassi et al.*, 2003]. The 1982 crater contains an acid (pH 2–3), warm (30°C), largely flat-bottomed (<4 m deep) green to whitish green-colored lake (Figure 2). Its volume is augmented by rainwater and by a chlorine-rich intermittent spring named "Soap Pool" (Figure 2). A progressive decrease in acidity, δD, and chlorine content of the crater lake and Soap Pool waters is explained by dilution with rainwater [*Rouwet et al.*, 2008]. However, significant variations in the volume of the lake do not reflect patterns of rainfall; instead, it is proposed to be related to the changes in circulation and recycling of hydrothermal waters [*Rouwet et al.*, 2008, 2009]. Among these parameters, the absence of a new source of Cl and a stable fumarolic activity, following an initial strong decrease immediately after the 1982 eruption, indicate the absence of reactivation of the magmatic system. Degassing sites are focused in a number of areas and segments of the crater, some being submerged by the lake. *Mazot and Taran* [2009] and *Mazot et al.* [2011] tentatively correlated alignments of degassing bubbles with the local and regional tectonic fabric. Weak trembling and earthquakes were felt during the field surveys, at a maximum rate of three to four per day, and are probably associated with phreatic activity in the partially sealed shallow aquifer [*Rouwet et al.*, 2009].

[12] The total heat flow from the volcano has been estimated at ~160 MW, with 20–43 MW from the crater lake itself. El Chichón geothermal system temperature at depth is estimated at 200–260°C and at ~200°C for the complete hydrothermal system [*Mazot et al.*, 2011; *Taran and Peiffer*, 2009; *Taran and Rouwet*, 2008].

2.3. Geology and Tectonic Setting

[13] El Chichón is part of the Transcurrent Fault Province of Chiapas [*García-Palomo et al.*, 2004], situated between two primarily calco-alkaline belts: the Trans-Mexican and the Central American volcanic belts. However, El Chichón has produced potassic-alkaline magmas [*Luhr et al.*, 1984] and is situated in a 450-km-long volcanic gap area. The surprising geochemical signature of El Chichón is explained by extensional tectonics associated with the triple junction between the North American, Caribbean, and Cocos plates according to *Nixon* [1982], although other authors proposed subduction of the Cocos plate under the North American plate [*Burbach et al.*, 1984; *Stoiber and Carr*, 1973].

[14] *Manea and Manea* [2008] proposed that the singular composition of El Chichón is related to the strong dehydration by deserpentinization of the subducting Tehuantepec Ridge, which triggered partial melting above the subducting slab. This situation of nonclassic arc tectonics is confirmed by $^{3}He/^{4}He$ isotopic ratios [*Mazot et al.*, 2011].

[15] The substrate of El Chichón is composed of Late Jurassic evaporates, Middle Cretaceous limestones, and Middle Miocene claystones and sandstones [*García-Palomo et al.*, 2004; *Layer et al.*, 2009, and references therein]. These sedimentary sequences are folded following the development of the Caimba and La Unión anticlines and the Buena Vista syncline. A complex of three faults system is developed and the maximum stress during the Late Miocene was in sinistral strike-slip, oriented N70°E.

3. Geomagnetic Field

3.1. Generalities

[16] The total magnetic intensity (TMI) on the Earth surface is affected by local variations of magnetic minerals (essentially magnetite). Characterization of mineralized buried structures (e.g., domes or dykes) or an absence of the minerals (e.g., fault, alteration zones, magma body, non-volcanogenic sediment) can be assessed by a geomagnetic survey [*Parasnis*, 1997]. Anomalies can be qualitatively interpreted or quantitatively modeled by forward modeling or inversion processes [*Li and Oldenburg*, 1996].

[17] Two main types of magnetic anomalies exist in volcanic areas: (1) induced magnetism, the temporary effect of the current magnetic field of the Earth on susceptible rocks; (2) remanent magnetism, which records the past magnetic field at the instant of the cooling of the volcanic rock [*Parasnis*, 1997]. The rocks of El Chichón are younger than 400 ka [*Layer et al.*, 2009] and hence we can confidently eliminate an influence of the remanent component.

3.2. Ground-Based Geomagnetic Survey

[18] Ground-based geomagnetic surveys were performed with a portable GSM-19 magnetometer (GEM Systems) in March and October 2007, collecting >70,000 data points over 3 km^2. Measurements were automatically recorded and positioned with a coupled GPS every 2 s. The local International Geomagnetic Reference Field (IGRF) has intensity 40,261 nT, declination D = 3°28′, and inclination I = 45°56′ at the moat (campsite; Figure 3). The Earth magnetic field intensity is transient and needs to be compensated when compiling different data sets. Thus the data need to be corrected for the secular variation if the surveys are spread over a long period of time. From the secular variation described by the IGRF model, 52 nT were added to the October 2007 data set for compilation with the values of March 2007. For this survey, a base station magnetometer was not employed and diurnal variations related to ionospheric and magnetospheric processes were assessed using a network of intermediate base stations on the crater floor. A maximum of 1 h was spent on each survey loop, and the diurnal variations were corrected if the variation exceeded 10 nT/h. The range of TMI recorded during the survey was very high (8,000 nT), and small issues with diurnal variations have little overall effect.

[19] Spacing in between tracks in the crater area is mostly <20 m. The lake area, which was surveyed from a small inflatable dinghy and the steep, unstable cliffs of the crater rim, were studied in less detail. However, the crater rim was climbed at various places and maximum horizontal distance in between these tracks is <150 m (Figure 3). Outside the crater rim, the surveys covered natural ridges, mounds, and

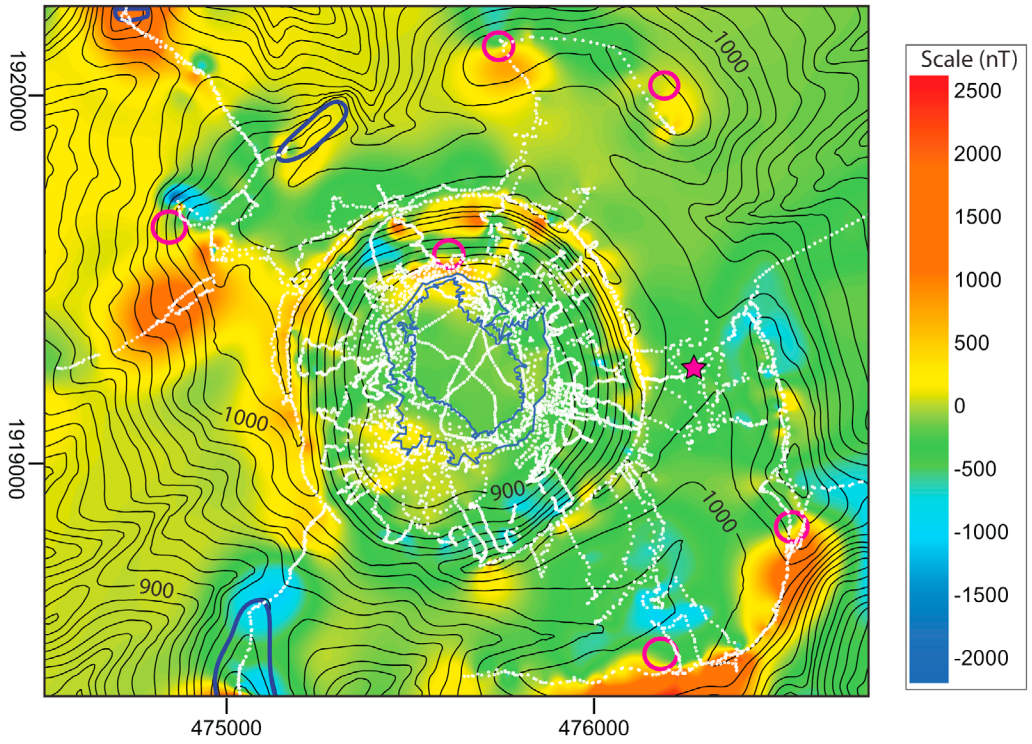

Figure 3. Ground-based residual geomagnetic intensity (in nT) of El Chichón, over topography (in m). White dots show survey tracks; thick blue lines for major cryptodome outcrops, magenta for minor outcrops, and star for campsite.

other accessible ground. Most of the outer volcano slopes and the moat area are impracticable for measurement, due to hundreds of steep dendritic gullies which dissected the 1982 deposits, now overgrown by thick vegetation.

[20] To assist in the interpretation of the TMI data, magnetic susceptibility (MS) was measured with an Exploranium handheld kappa meter on the surfaces of a wide variety of fresh and altered material.

3.3. Geomagnetic Inversions

[21] Inversion of the TMI data set was undertaken with the UBC-GIF software which solves for a three-dimensional discretized magnetic susceptibility model of the subsurface by simultaneously minimizing a data misfit function and a model objective function that favors "small" and "smooth" models [*Li and Oldenburg*, 1996]. We completed an inversion of the ground-based TMI in the lower crater area using a model which incorporated the form of the local topography. The ground magnetic data were upward continued for 20 m prior to inversion to eliminate the very high-frequency anomalies related to surficial susceptibility variations. Although the magnetic data were corrected to residual anomalies by removal of the IGRF intensity, an additional DC offset of +180 nT was added to the residual data set prior to inversion to match the data set with the regional positive anomaly associated with large-scale bodies emplaced around the volcano (see below). The resulting residual TMI data set had a range of over 900 nT and was inverted into a cubic, 700-m-long, 5-m-spaced voxel mesh at the surface.

[22] To provide a more regional view of major magnetic sources, we also digitized the TMI data for an area of 14 × 15.3 km centered on the volcano, from a contour map of TMI derived from a regional airborne geomagnetic survey with 1 km-spaced lines [*Servicio Geológico Mexicano*, 2006]. This data set is upward continued for 300 m above topography and spreads over >600 nT. The voxel mesh employed for this inversion was 100 × 100 m in easting and northing, with a vertical cell dimension of 20 m at the surface, which increased to 100 m at 2.5 km depth. The large Neogene granodiorite-diorite intrusion of Santa Fe <20 km to the east [*Damon and Montesinos*, 1978] forms a major magnetic anomaly which slightly overlaps the one centered on El Chichón. Nevertheless, the influence of this magnetic anomaly could be characterized and subtracted from the El Chichón data.

3.4. Results

3.4.1. Ground-Based Geomagnetic Survey

[23] The local TMI map shows multiple magnetic anomalies spread over El Chichón volcano (Figure 3) together with the distribution of magnetic observations. Magnetic field variations are reasonably well sampled on the crater floor but on the dissected flanks of the volcano the data are sparse and anomalies are almost certainly aliased. Most of the anomalies have a strong positive component and are found on the somma crater rim or just outside of the 1982 crater. Initial interpretation focused on qualitative interpretation of the position and relative depth of the magnetic bodies and correlations with field observations. Four high-

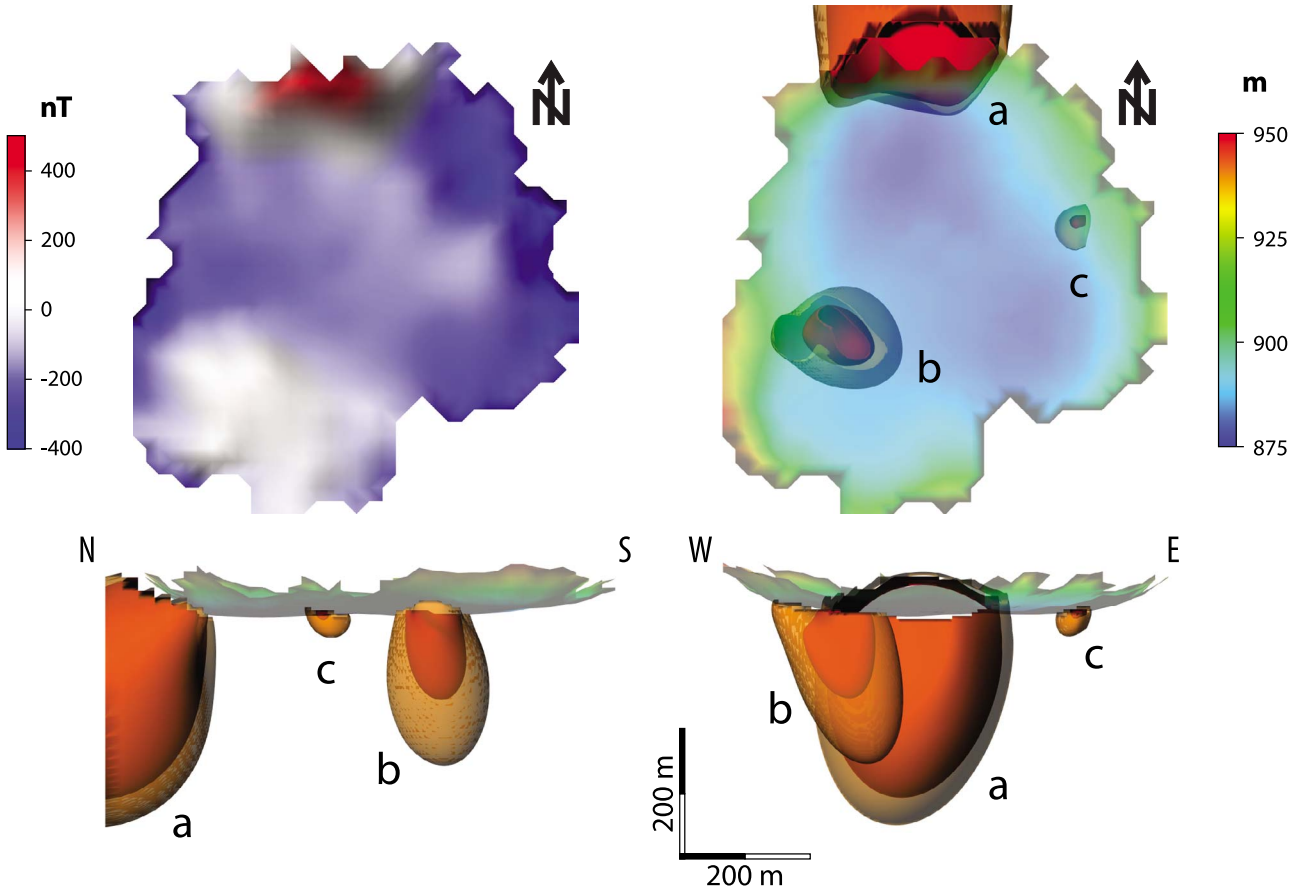

Figure 4. (top left) Ground-based residual magnetic intensity of the crater floor upward continued by 20 m height; scale in nT. (top right) Top view of the crater floor topography with isosurfaces of the 3-D inversion model at 0.025 and 0.033 SI. (bottom) Lateral views of isosurfaces from the 3-D inversion model showing the three anomalies (*a*, *b*, and *c*) discussed in the text. (left: N-S; right: W-E).

intensity anomalies were detected and three of them correspond to major structures: the NW "dome," SW "dome," and SE summit (Figure 2). The fourth anomaly is centered on the top of the western ridge of the volcano. Many smaller anomalies are situated around the two craters, and many of them correspond to visible outcrops of lava domes or cryptodomes. Magnetic susceptibility generally correlates with sample size and alteration state. Highest values (0.02 to 0.04 SI) were found for blocks and cobbles associated with the domes, whereas random pebbles were lower (<0.02 SI); altered surfaces, clays, and fine-grained volcaniclastic sediments were usually <0.001 SI. Thus the more coherent dome material is comparatively strongly magnetized, whereas smaller rocks, usually more altered and weathered, are weakly magnetized or effectively nonmagnetic.

[24] In the 1982 crater floor area, three TMI anomalies were detected and were successfully inverted in 3-D as illustrated by the 0.025 and 0.033 magnetic susceptibility isosurfaces shown in Figure 4. The causative bodies for the three anomalies (labeled *a*, *b*, and *c*) are resolved as effectively vertical ellipsoids, with a maximum inferred depth extent of ~300 m (anomaly *a*) and 120 to 250 m (anomaly *b*), whereas anomaly *c* is more superficial (<50 m).

3.4.2. Aeromagnetic Survey

[25] The 3-D inversion of the airborne TMI highlighted four major anomalies around the 1982 crater, in addition to minor anomalies outside the studied area (Figure 5). The absence of a significant regional magnetic anomaly in the center of the 1982 crater is remarkable. The relatively wide-spacing and large effective terrain clearance of the airborne survey provide a low-pass filtered view of the TMI, which effectively suppresses high-frequency anomalies due to near surface features and highlights more regional components. Three of the major anomalous bodies from the regional inversion correspond to the three largest anomalies of the ground-based TMI: SE summit, NW dome, and SW dome. The area of the anomaly to the W and the eastern part of the SE summit was not covered by the ground-based survey. The subsurface morphology of the inverted anomalous bodies is illustrated in Figure 6 by the MS isosurfaces (0.023, 0.033, 0.042, 0.047, and 0.060 SI).

4. Very Low Frequency EM

4.1. Methodology

[26] Very low frequency (VLF) waves (15–25 kHz) are generated from several emitters around the world for sub-

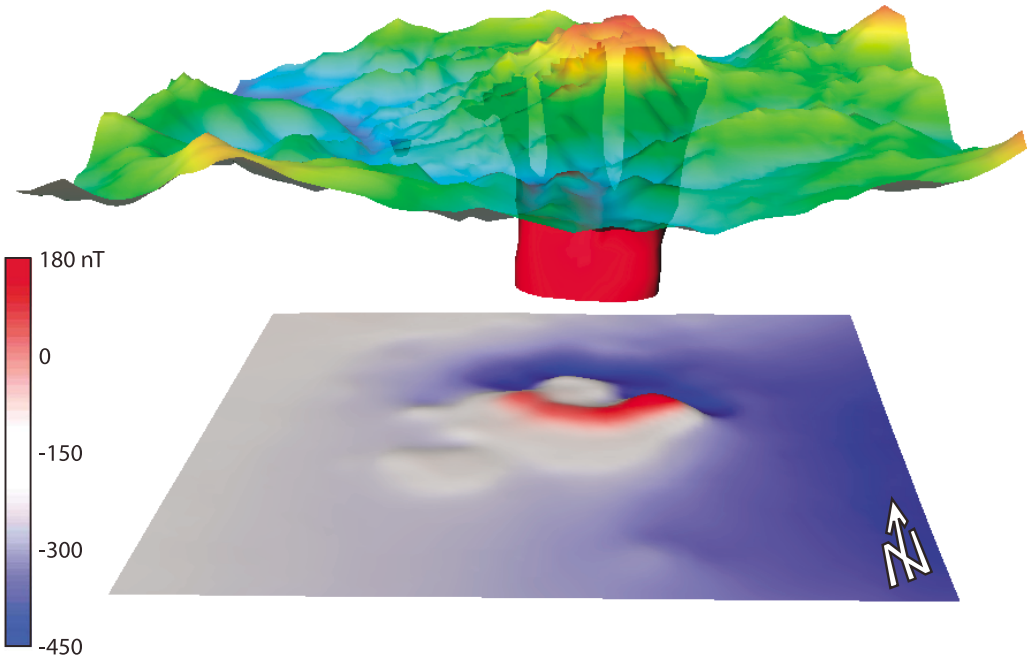

Figure 5. Inversion model in 3-D of the aeromagnetic data set. (bottom) Residual magnetic intensity anomaly, digitized from an aeromagnetic data set, at a virtual height of 300 m above topography, scale in nT. (top) Topography and isosurface of the 3-D inversion model (red) with a magnetic susceptibility of 0.033. Total area is 14 × 15.3 km, northward view, slight tilt to the north, vertical exaggeration of 2.5.

marine communication, but these powerful, constant, and widespread electromagnetic waves can also be used for peaceful purposes. We used a portable VLF receiver to detect electric anomalies in the shallow surface of the 1982 crater. Fumaroles contain metallic ions which are deposited in the fractures at the near surface, and the high water acidity contributes to the dissolution of the wall rock and accumulation of clays around the vents. Thus a highly conductive response is expected for extinct and active hydrothermal vents [*Zablocki*, 1978]. When the vent is active and connected to the hydrothermal system, it will be saturated with highly conductive water.

[27] In response to the primary VLF horizontal magnetic field, an induced electrical current is generated within a (buried) conductive body. A secondary magnetic field is then generated at the same frequency by this electrical current but oriented now vertically. The dip angle between the horizontal magnetic vector and the resultant vector (primary + secondary) is the value studied with VLF instruments [*McNeill and Labson*, 1991]. VLF surveys were performed using a portable GSM-19 (GEM Systems), recording three bands (frequencies) simultaneously. Seattle was the most reliable and powerful emitter, thus we focus on its data in this paper. Raw VLF data sets can be complex to analyze directly, and a standard filtering process is commonly used. We used the software KHFFILT 1.1a [*Pirttijärvi*, 2004] to apply the *Karous and Hjelt* [1983] filter, which reduces potential topographic anomalies and transforms the dip angle of the in-phase values into well-defined unitless peaks. After filtering, positive anomalies represent conductive bodies (saturated sediment, mineralization, clay), whereas negative anomalies correspond to more resistant bodies such as massive rock or unsaturated sediment. Anomalies can be qualitatively defined in terms of their vertical and horizontal extent, as well as their approximate angle of dip.

4.2. Results

[28] A total of 38 VLF transects were completed in the crater during November 2006, March 2007, and October 2007 campaigns (Figure 7). Measurements were made every 5 m, facing north; the overall flat topography (<10 m of variation) of the crater floor ruled out any complication due to topographic anomalies. Numerous local dipping anomalies were detected on every transect.

[29] The unaltered rock on the crater floor has a rather homogeneous chemical and primary mineralogical composition, but the range of porosity and water saturation is large, and that variation together with the presence of clays result in significant contrasts in resistivity. The mostly trachy-andesitic composition of the rocks of El Chichón should approximate to 100–1,000 ohm·m [*Milsom*, 1996], and this corresponds to an investigation skin depth of 30–100 m. Lack of resistivity measurements prevents more constrained values of the skin depth, as well as accuracy in the vertical scale of the pseudosections [*McNeill and Labson*, 1991; *Milsom*, 1996]. The presence of water strongly increases the ground conductivity; thus it should significantly affect the VLF signal. For example, the strong anomalies detected in section 1 may be related to presence of a shallow water table, as this transect crossed a flat, water-saturated alluvial fan on the southern lake shore.

[30] For a better visualization of the results, the data from two depths were extracted from the pseudosections and

complied into two pseudomaps (Figure 8). Considering the value of the skin depth at 30–100 m, the two maps theoretically correspond to 5 m and 15 m depth. The advantage of these pseudomaps is that they show the lateral and ver-

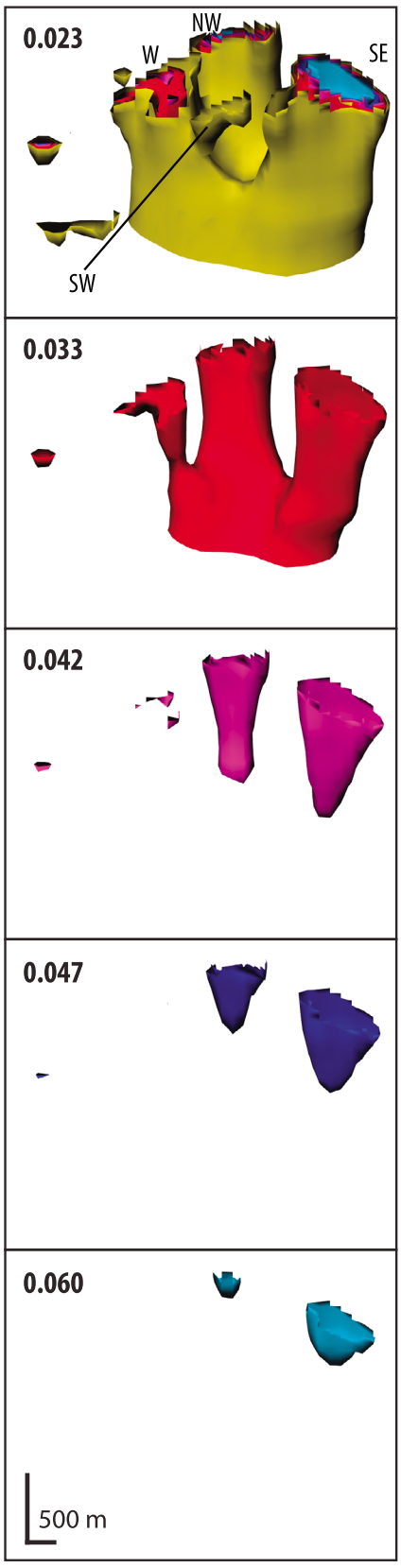

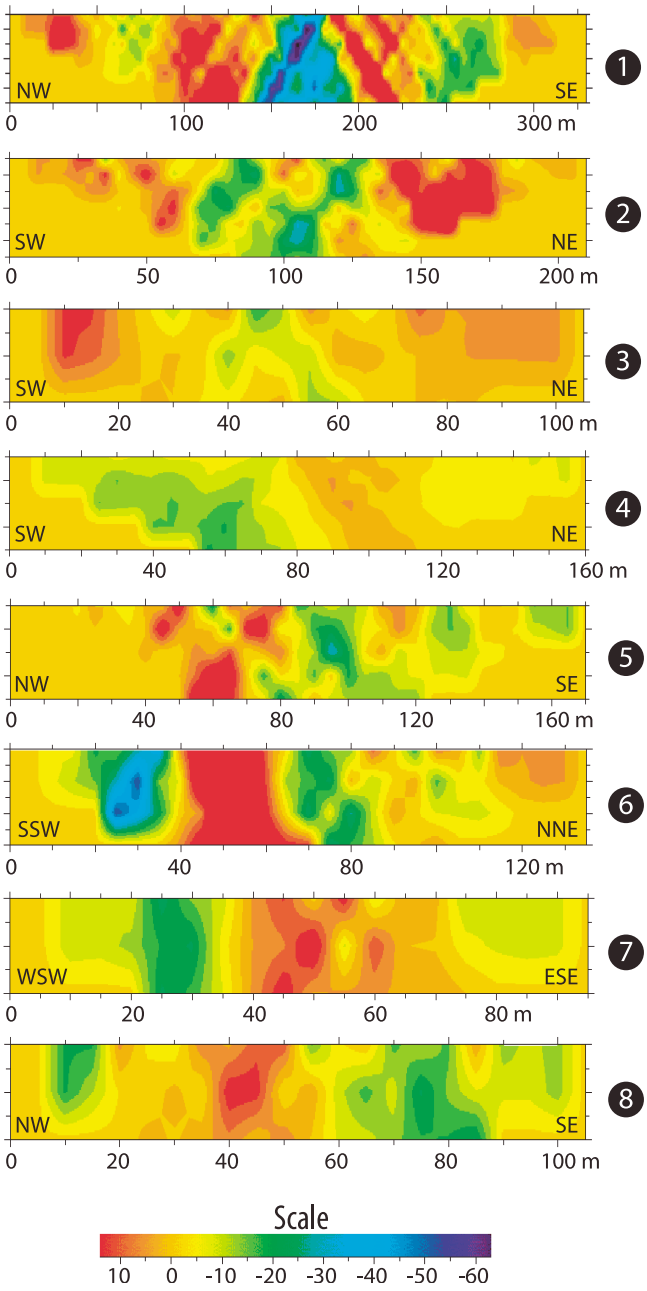

Figure 7. Selected very low frequency (VLF) pseudosections of the crater floor. Data filtered following *Karous and Hjelt* [1983]. See Figure 8 for corresponding tracks. Cross section built with KHFFILT 1.1a [*Pirttijärvi*, 2004].

Figure 6. Isosurfaces derived from the 3-D inversion model of the aeromagnetic anomaly. The features are truncated by topography at their upper surface. Five susceptibilities isosurfaces are represented: 0.023 SI (yellow), 0.033 SI (red), 0.042 SI (magenta), 0.047 SI (blue), and 0.060 SI (light blue). The four major anomalies (NW, SW, SE, and W) highlight highly magnetized cryptodomes or intrusions around the 1982 crater. Northward view, tilt of 45° to the north, vertical exaggeration of 2.5.

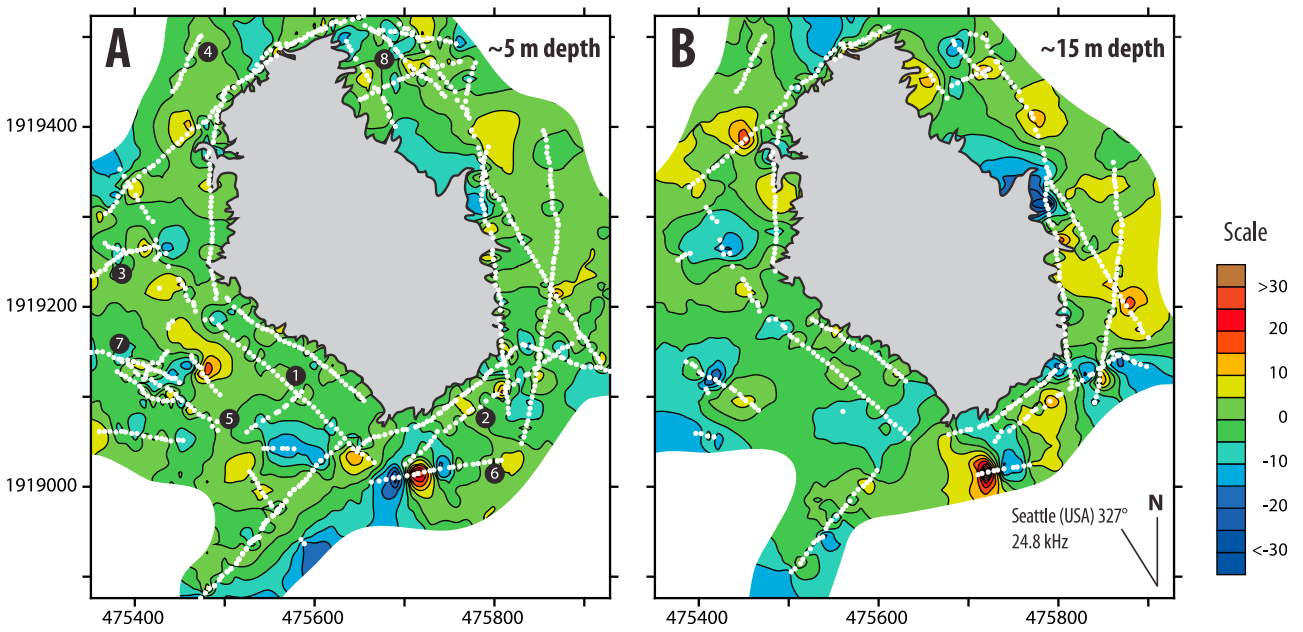

Figure 8. VLF pseudomaps, showing anomalies at depth of (a) 5 m and (b) 15 m. In gray, lake shape from October 2007; white dots refer to measured stations; numbers refer to cross sections of Figure 7. Orientation of the Seattle emitter mentioned.

tical extent of each anomaly, although the small extent of the surveys (hundreds of meters) implies that the deeper pseudomap (15 m, Figure 8b) is constrained by less data than the shallow pseudomap (5 m, Figure 8a) at its extremities. Localized positive (conductive) and negative (resistive) anomalies are apparent in the pseudosections and pseudodepth maps, many of which appear to extend to depth. The biggest negative anomaly is found at the northeastern shore, within the main hydrothermal area, but where 10-m high ridges are present.

5. Interpretation and Discussion

5.1. Magnetized Bodies

5.1.1. Identification of the Magnetic Bodies

[31] The magnetic susceptibility of the extrusive dome material is very high, resulting in TMI anomalies that are easily identifiable over the low magnetic regional background (Figure 5). The morphology of the visible "NW dome" (90 ka) and "SW dome" (217 ka) [*Layer et al.*, 2009] together with the 3-D aeromagnetic inversion are not consistent with classical models of recently erupted trachyandesitic domes, which show a much flatter aspect ratio and an absence of deep roots [*Fink and Griffiths*, 1998]. The zone of very high subsurface magnetic susceptibility inferred from inversion of the aeromagnetic data largely exceeds the now visible >200 m high cliffs of the massive NW and SW "domes" (Figures 2 and 6).

[32] The surface exposures of the NW dome and SE summit correspond closely with the 0.060 SI isosurface from the 3-D aeromagnetic inversion, whereas outcrops of the SW dome coincide with the 0.023 SI isosurface, suggesting variability in the degree of magnetization of the different intrusive bodies. These susceptibility values have been utilized to infer the likely subsurface geometry of each body from the 3-D inverse volume. On this basis, the NW and SE domes are inferred to taper downward with a maximum depth extent of approximately 500 m. The maximum depth extent of the SW dome is interpreted to be <200 m. No prominent topography is visible above the area of the E anomaly, which suggests small-scale bodies at a relatively high susceptibility (e.g., 0.042) at depth not deeper than <200 m. We propose that the highly magnetized, deeply rooted bodies were emplaced within the complex of El Chichón volcano as shallow intrusions, such as cryptodomes. The uppermost volume of these cryptodomes was possibly extrusive. The modeled depth and horizontal projection of the susceptibility isosurfaces gives an aspect ratio of ~0.2 to 0.5, which corresponds to the shape of a vertical intrusion (Figure 6).

[33] On the basis of old photographs, *Duffield et al.* [1984] depicted the area around the SW "dome" as a crater rim and *Layer et al.* [2009] described that the somma crater had been "disturbed" by emplacement of the "SW dome." We propose this contact to be better explained by emplacement of an intrusive body. Large ridges and topographic depressions are formed around the two NW and SW cryptodomes, whereas the SE summit rims the Guayabal tuff cone [*Layer et al.*, 2009]. These remarkable topographic features are interpreted here as remnants of crater rims, or collapse scars relating to small sector collapses, associated with the growth of the intrusive bodies [*Donnadieu et al.*, 2001].

[34] Absence of a large-scale positive magnetic anomaly centered in the middle of the 1982 crater suggests that most of the 550 BP nested dome was pulverized during the last eruption. It also confirms that a large resurgent dome or cryptodome is not associated with the 1982 eruption.

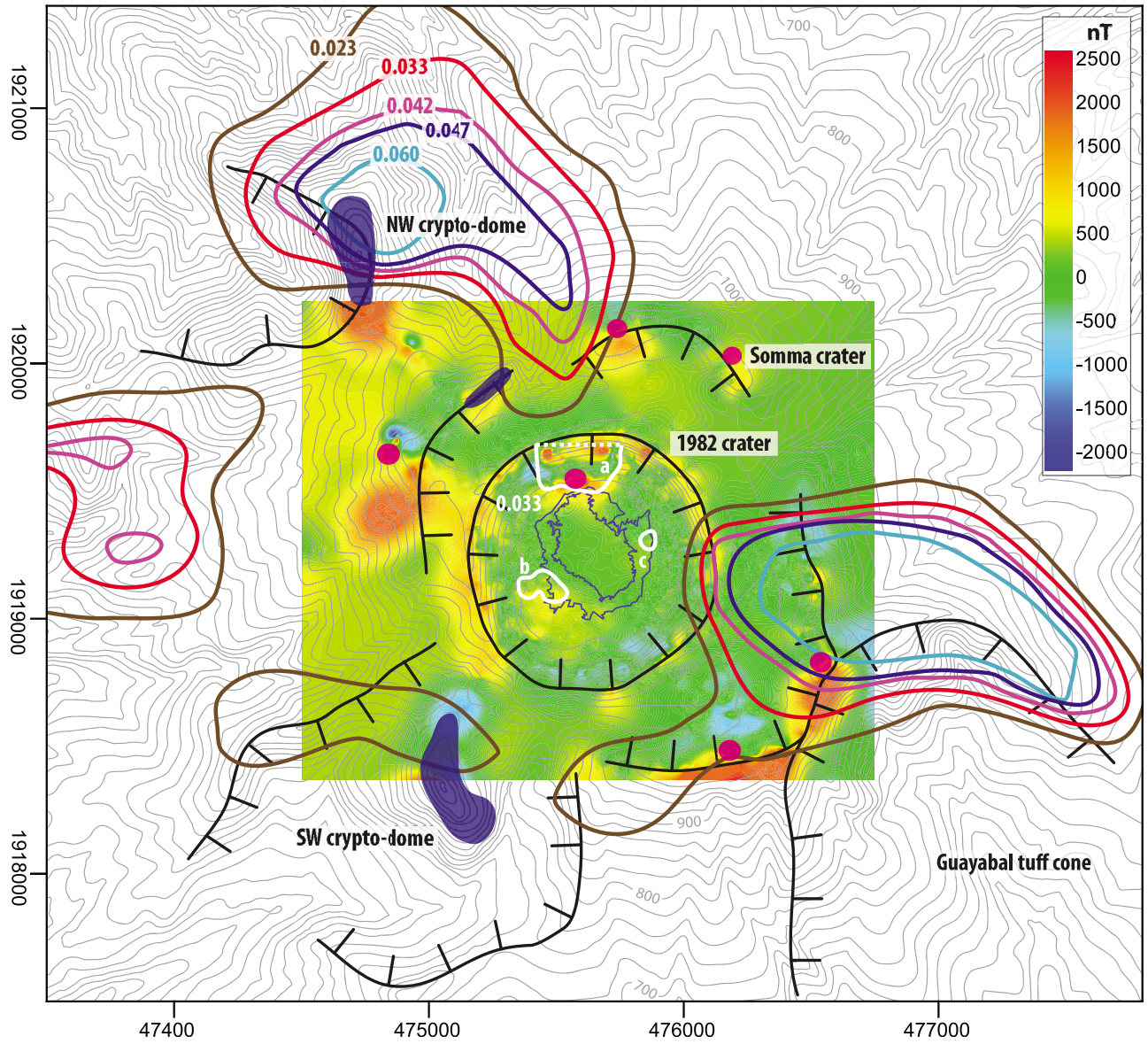

Figure 9. Generalized interpretation of the morphology and structure at the summit of El Chichón volcano. Ground-based residual anomaly colored map (in nT); topography as gray contour lines (10 m spacing). Craters and deep collapse scars highlighted in black lines. Large outcrops of massive cryptodomes are in dark blue patches, and minor dome rock remnants are in magenta. Thick colored lines are the traces of isosurfaces from the 3-D aeromagnetic inversion on the topography with magnetic susceptibility at 0.023 (brown), 0.033 (red), 0.042 (purple), and 0.060 (light blue). Traces of the 0.033 SI susceptibility isosurfaces from inversion of ground-based TMI data are shown in white.

[35] We interpret the small magnetized bodies *a*, *b*, and *c* confined to the 1982 crater as mostly associated to remnants of the 550 BP dome roots, which were almost completely destroyed by the last eruption (Figure 9). At the site of anomaly *a*, a massive outcrop of highly magnetized dome is visible at the base of the crater wall, as well as a recent-looking (1982?) dyke discovered in the field (Figure 2). This dyke (185/70) is ~5 m long, <30 cm thick, is surrounded by fumaroles, and shows striations with a pitch of 20° toward the W, interpreted as being formed during the last movement of the magma. Its position corresponds to the westernmost side of the anomaly *a*.

[36] The various small outcrops of dome rocks on the eastern summit and possibly northern ridge were interpreted as alignment of domes by *Rose et al.* [1984]. The high amplitude and short wavelength of the magnetic anomalies associated with these bodies on the ground-based map, as well as the small extent of outcrops in the field are here interpreted to be possible surficial exposures of either (1) parts of major cryptodomes (e.g., E summit), (2) remnants of small domes/plugs or their associated talus breccia [*Macías et al.*, 2003], (3) remobilized slabs and blocks associated with old domes or plugs destroyed by younger eruptions, or (4) local lava flow associated to the 500 BP

dome on the W of the 1982 crater [*Macías et al.*, 2007]. We stress that the short wavelength of the geomagnetic anomalies attests to the surficial nature of these structures (Figure 3). Similarly, the semicontinuous positive anomaly around the 1982 crater rim is probably related to remnants of the well-developed vertical cliffs of the 550 BP dome talus breccia buried under the recent deposits [*Rose et al.*, 1984] or by a lava flow on the W side [*Macías et al.*, 2007].

5.1.2. New Dome Growth

[37] The possibility of a future dome growth within the 1982 crater has been proposed based on the presence of multiple massive "domes" present within the volcanic edifice and a large dome emplaced after the 550 BP eruption [*Macías et al.*, 2003; *Rouwet et al.*, 2008; *Taran et al.*, 2008]. However, the stratigraphic record suggests that at least 11 eruptions have occurred within the somma crater during the last 8000 years and that several of them, including the 550 BP, did not destroy big domes [*Espíndola et al.*, 2000; *Macías et al.*, 2003]. Moreover, the lateral Guayabal tuff cone does not contain a visible dome. Delayed growth of a dome or cryptodome may happen in the near future, as seen in many other volcanoes [see *Rouwet et al.*, 2008], but remains uncertain for El Chichón volcano.

5.2. Hydrothermal System

5.2.1. Total Magnetic Intensity

[38] The hydrothermal system of El Chichón is composed of the pre-1982 heat source [*Canul et al.*, 1983; *Damon and Montesinos*, 1978; *Mulleried*, 1933], overprinted by the new 1982 magmatic input [*Rouwet et al.*, 2008; *Taran et al.*, 2008]. The size of aquifers beneath the crater are undoubtedly significant, as indicated by the constant discharge of >300 l/s of water at ~70°C at thermal springs on the flanks of the volcano, in addition to the Soap Pool in the 1982 crater [*Rouwet et al.*, 2008; *Taran and Peiffer*, 2009; *Taran et al.*, 2008]. The magnetic intensity of the three bodies beneath the crater floor is high enough to prevent detection of possible negative anomalies associated to rocks demagnetized by hydrothermal alteration, saturated porous rocks, or faults [*García-Palomo et al.*, 2004; *Mazot et al.*, 2011].

[39] The three magnetic anomalies detected on the 1982 crater floor, and which are interpreted as remnants of old dome complexes, correspond to the most hydrothermally active areas in the crater (Figures 2 and 9). This strongly suggests that, despite their age, the 550 BP dome remnants seem to be the main source of heat of the lake-spring hydrothermal system, and still hot enough to generate boiling fluids. The altitude of the thermal springs on the southern and western flanks of the volcano is 700–750 masl. This matches the modeled basal depth of the closest magnetic body (anomaly *b*), which has maximum depth of 250–120 m, corresponding to 610–740 masl.

[40] Presence of old massive dome rocks in the area of anomaly *a* (Figure 2) and witnessed hydrothermal activity in the moat area and at the flank springs well before the 1982 eruption [*Canul et al.*, 1983; *Mulleried*, 1933; *Templos*, 1981] indicate that the last volcanic eruption is not the main driving component of the current hydrothermal systems of El Chichón. However, the regular asymptotic decrease of the Cl concentration in the soap pool since the 1982 eruption [*Rouwet et al.*, 2004, 2008, 2009] and absence of a magnetized body beneath it suggest that it is associated with a hydrothermal cell formed after this eruption. The magnetic anomaly *c* matches the most powerful fumarole field of the crater and might feed the soap pool, despite its situation 200 m to the SE. This would indicate that the anomaly *c* might be a small degassed remnant of magma emplaced at shallow depth during the last stage of the 1982 eruption.

5.2.2. Very Low Frequency EM

[41] The two VLF pseudomaps show a highly irregular conductivity distribution with no well-constrained lineaments. Positive EM anomalies are noticeably centered on active and extinct fumarole fields. Sulfur and sinter deposits and abundance of clays characterize hydrothermal fields, active or extinct. We considered the field active when visible heat and/or fumaroles were present. On the western shore and to the south, numerous sites were considered extinct. Most of the positive VLF anomalies are directly related to hydrothermal vents and local fractures. Negative VLF anomalies were found on stratified topographic mounds composed of postclimatic phreatomagmatic surge deposits (Figure 2), well above the vadose zone, such as on the northeastern shore of the crater lake. They also indicate a possible presence of faults [*Mazot and Taran*, 2009] not connected to the hydrothermal system, thus less conductive.

5.2.3. Field Evidence

[42] Careful examination of photos taken in June 1982 confirmed that changes in the crater morphology were minimal between June 1982, late 1982 (date of creation of the geological map by *Rose et al.* [1984]), and the present time. The three primitive lakes were formed within multiple explosion pits inside the phreatomagmatic deposits of 4 April to May 1982 [*Tilling*, 1982, 2009; R. I. Tilling, personal communication, 2010]. The strong similarity between the morphology of several ridges from the photos of June 1982, the map of November 1982 [*Rose et al.*, 1984], and the current outcrops indicate that the crater floor has been at the same altitude (i.e., 860 m) since the end of the climactic eruption of early April 1982. Significant changes are: minor collapses of the crater wall (June 1982 to present), destruction of the central ridges delimitating the three lakes by phreatic explosions (September 1982), creation of a single lake by the same phreatic activity, and partial resedimentation of the phreatomagmatic deposits in alluvial fans by rain erosion (June 1982 to present). Therefore the crater lake(s) have always been at essentially the same elevation, which contradicts the hypothesis of an initial deeper crater lake, buried by ~100 m thick breccia associated with the collapse of unstable crater walls during the year 1982–1983 [*Casadevall et al.*, 1984]. Thus we propose that the initially very acid and chlorine-rich waters from the "shallow boiling aquifer" of *Rouwet et al.* [2008] are not related to a "1982 buried lake" but to the contact of the water table with brecciated remnants of the still-hot 550 BP dome and its associated hydrothermal system.

6. Conclusions

[43] A multidisciplinary geophysical survey was carried out on El Chichón volcano (Chiapas, Mexico) during November 2006 and March and October 2007. We delineated the internal structures of the volcanic edifice, as well

as the surficial manifestations of the associated hydrothermal system. Three ground-based geomagnetic anomalies beneath the 1982 crater were inverted in 3-D and their positions correspond to the most active hydrothermal fields in the crater. Inverted magnetic susceptibility and field evidence strongly suggest they correspond to highly magnetized remnants of the 550 BP dome. The maximum basal depth of these anomalies matches the elevation of thermal springs on the flank of the volcano. Witnessed hydrothermal activity before 1982, and presence of old massive dome rocks in the area of anomaly *a* (Figure 2) indicate that the hydrothermal system of El Chichón volcano was established well before the last eruption. Despite its large regional and worldwide impact, the 1982 eruption had little effect on its deep hydrothermal system and did not affect the discharge of water in the flank springs, although possibly intruding a small magnetic body (anomaly *c*) in its crater, which represents a possible heat source for the Cl-rich waters of the soap pool situated in the newly formed crater. Four major, deeply rooted, carrot-shaped cryptodome intrusions were depicted from a 3-D inversion of an aeromagnetic data set, and correspond to the E summit, and the NW and SW "domes."

[44] The shallow structure of the 1982 hydrothermal system was characterized by a VLF survey. The active and extinct fumarole vents of the crater floor are grouped in several areas of intense fumarolic activity but are also scattered in multiple isolated spots. In contrast to the CO_2 degassing of the crater lake, the fumarole vent pattern does not show clear lineaments but follows the modeled magnetic anomalies. Examination of posteruption photos shows that the crater morphology underwent only minor modifications since the end of the climactic 1982 eruption and that the crater floor has always been at the same altitude since then.

[45] **Acknowledgments.** Thanks to Dmitri Rouwet for fruitful collaboration in the field, encouraging discussions, and manuscript review. Editor A. Revil and reviewer J. L. Macías improved the manuscript. Thanks also to H. Carter and A. Mazot for assistance in the field, R. Tilling for access to his photos of 1982, and the Sanchez family for field logistic. This project was partially funded by the CONACYT grant to NV (41199).

References

Araña, V., A. G. Camacho, A. Garcia, F. G. Montesinos, I. Blanco, R. Vieira, and A. Felpeto (2000), Internal structure of Tenerife (Canary Islands) based on gravity, aeromagnetic and volcanological data, *J. Volcanol. Geotherm. Res.*, *103*, 43–64, doi:10.1016/S0377-0273(00)00215-8.

Blanco-Montenegro, I., R. Ritis, and M. Chiappini (2007), Imaging and modelling the subsurface structure of volcanic calderas with high-resolution aeromagnetic data at Vulcano (Aeolian Islands, Italy), *Bull. Volcanol.*, *69*, 643–659, doi:10.1007/s00445-006-0100-7.

Burbach, G. V., C. Frohlich, W. D. Pennington, and T. Matumoto (1984), Seismicity and tectonics of the subducted Cocos Plate, *J. Geophys. Res.*, *89*, 7719–7735, doi:10.1029/JB089iB09p07719.

Canul, R. F., M. A. Razo, and V. L. Rocha (1983), Geología e historia volcanólgica del Volcán Chichonal, Estado de Chiapas (Geology and volcanic history of El Chichon Volcano), pp. 3–22, Rev. del Inst. de Geol., Chiapas, Mexico.

Carey, S., and H. Sigurdsson (1986), The 1982 eruptions of El Chichón volcano, Mexico (2), Observations and numerical modelling of tephra-fall distribution, *Bull. Volcanol.*, *48*, 127–141, doi:10.1007/BF01046547.

Casadevall, T. J., S. De La Cruz-Reyna, W. I. Rose Jr., S. Bagley, D. L. Finnegan, and W. H. Zoller (1984), Crater lake and post-eruption hydrothermal activity, El Chichón volcano, Mexico, *J. Volcanol. Geotherm. Res.*, *23*, 169–191, doi:10.1016/0377-0273(84)90061-1.

Cassidy, J., S. J. France, and C. A. Locke (2007), Gravity and magnetic investigation of maar volcanoes, Auckland volcanic field, New Zealand, *J. Volcanol. Geotherm. Res.*, *159*, 153–163, doi:10.1016/j.jvolgeores.2006.06.007.

Damon, P. E., and E. Montesinos (1978), Late Cenozoic volcanism and metallogenesis over an active Benioff zone in Chiapas, Mexico, *Ariz. Geol. Soc. Dig.*, *11*, 155–168.

De Ritis, R., G. Ventura, and M. Chiappini (2007), Aeromagnetic anomalies reveal hidden tectonic and volcanic structures in the central sector of the Aeolian Islands, southern Tyrrhenian Sea, Italy, *J. Geophys. Res.*, *112*, B10105, doi:10.1029/2006JB004639.

Donnadieu, F., O. Merle, and J. C. Besson (2001), Volcanic edifice stability during cryptodome intrusion, *Bull. Volcanol.*, *63*, 61–72, doi:10.1007/s004450000122.

Duffield, W. A., R. I. Tilling, and R. Canul (1984), Geology of El Chichón volcano, Chiapas, Mexico, *J. Volcanol. Geotherm. Res.*, *20*, 117–132, doi:10.1016/0377-0273(84)90069-6.

Espíndola, J. M., J. L. Macías, R. I. Tilling, and M. F. Sheridan (2000), Volcanic history of El Chichón Volcano (Chiapas, Mexico) during the Holocene, and its impact on human activity, *Bull. Volcanol.*, *62*, 90–104, doi:10.1007/s004459900064.

Fink, J. H., and R. W. Griffiths (1998), Morphology, eruption rates, and rheology of lava domes: Insights from laboratory models, *J. Geophys. Res.*, *103*, 527–545, doi:10.1029/97JB02838.

Finn, C. A., T. W. Sisson, and M. Deszcz-Pan (2001), Aerogeophysical measurements of collapse-prone hydrothermally altered zones at Mount Rainier volcano, *Nature*, *409*, 600–603, doi:10.1038/35054533.

Finn, C. A., M. Deszcz-Pan, E. D. Anderson, and D. A. John (2007), Three-dimensional geophysical mapping of rock alteration and water content at Mount Adams, Washington: Implications for lahar hazards, *J. Geophys. Res.*, *112*, B10204, doi:10.1029/2006JB004783.

García-Palomo, A., J. L. Macías, and J. M. Espíndola (2004), Strike-slip faults and K-alkaline volcanism at El Chichón volcano, southeastern Mexico, *J. Volcanol. Geotherm. Res.*, *136*, 247–268, doi:10.1016/j.jvolgeores.2004.04.001.

Hildenbrand, T. G., J. G. Rosenbaum, and J. P. Kauahikaua (1993), Aeromagnetic study of the Island of Hawaii, *J. Geophys. Res.*, *98*, 4099–4119, doi:10.1029/92JB02483.

Hurst, A. W., P. C. Rickerby, B. J. Scott, and T. Hashimoto (2004), Magnetic field changes on White Island, New Zealand, and the value of magnetic changes for eruption forecasting, *J. Volcanol. Geotherm. Res.*, *136*, 53–70, doi:10.1016/j.jvolgeores.2004.03.017.

Karous, M., and S. E. Hjelt (1983), Linear filtering of VLF dip-angle measurements, *Geophys. Prospect.*, *31*, 782–794, doi:10.1111/j.1365-2478.1983.tb01085.x.

Krueger, A., N. Krotkov, and S. Carn (2008), El Chichón: The genesis of volcanic sulfur dioxide monitoring from space, *J. Volcanol. Geotherm. Res.*, *175*, 408–414, doi:10.1016/j.jvolgeores.2008.02.026.

Layer, P. W., A. García Palomo, D. Jones, J. L. Macías, J. L. Arce, and J. C. Mora (2009), El Chichon volcanic complex, Mexico; stages of evolution based on field mapping and $^{40}Ar/^{39}Ar$ geochronology, *Geofis. Int.*, *48*, 33–54.

Lénat, J. F., and M. Aubert (1982), Structure of Piton de la Fournaise volcano (La Réunion Island, Indian Ocean) from magnetic investigations. An illustration of the analysis of magnetic data in a volcanic area, *J. Volcanol. Geotherm. Res.*, *12*, 361–392, doi:10.1016/0377-0273(82)90035-X.

Li, Y., and D. W. Oldenburg (1996), 3-D inversion of magnetic data, *Geophysics*, *61*, 394–408, doi:10.1190/1.1443968.

Luhr, J. F., I. S. E. Carmichael, and J. C. Varekamp (1984), The 1982 eruptions of El Chichón volcano, Chiapas, Mexico: Mineralogy and petrology of the anhydrite-bearing pumices, *J. Volcanol. Geotherm. Res.*, *23*, 69–108, doi:10.1016/0377-0273(84)90057-X.

Macías, J. L., M. F. Sheridan, and J. M. Espíndola (1997), Reappraisal of the 1982 eruptions of El Chichón Volcano, Chiapas, Mexico: New data from proximal deposits, *Bull. Volcanol.*, *58*, 459–471, doi:10.1007/s004450050155.

Macías, J. L., J. L. Arce, J. C. Mora, J. M. Espíndola, R. Saucedo, and P. Manetti (2003), A 550-year-old Plinian eruption at El Chichón Volcano, Chiapas, Mexico: Explosive volcanism linked to reheating of the magma reservoir, *J. Geophys. Res.*, *108*(B12), 2569, doi:10.1029/2003JB002551.

Macías, J. L., J. L. Arce, T. Scolamacchia, D. Rouwet, A. García, J. M. Espíndola, and Y. Taran (2007), El Chichón volcano, paper presented at El Chichón Volcano: Twenty-Five Years Later. A Commemorative Conference, Univ. Nac. Auton. de Mexico, Chiapas, Mexico.

Macías, J. L., L. Capra, J. L. Arce, J. M. Espíndola, A. García-Palomo, and M. F. Sheridan (2008), Hazard map of El Chichón volcano, Chiapas, México: Constraints posed by eruptive history and computer simulations, *J. Volcanol. Geotherm. Res.*, *175*, 444–458, doi:10.1016/j.jvolgeores.2008.02.023.

Manea, M., and V. C. Manea (2008), On the origin of El Chichón volcano and subduction of Tehuantepec Ridge: A geodynamical perspective, *J. Volcanol. Geotherm. Res.*, *175*, 459–471, doi:10.1016/j.jvolgeores.2008.02.028.

Mazot, A., and Y. Taran (2009), CO_2 flux from the volcanic lake of El Chichón (Mexico), *Geofis. Int.*, *48*, 73–83.

Mazot, A., D. Rouwet, Y. Taran, S. Inguaggiato, and N. R. Varley (2011), CO_2 and He degassing at El Chichón volcano, Chiapas, Mexico: Gas flux, origin, and relationship with local and regional tectonics, *Bull. Volcanol.*, doi:10.1007/s00445-010-0443-y, in press.

McNeill, J. D., and V. F. Labson (1991), Geological mapping using VLF radio fields, in *Electromagnetic Methods in Applied Geophysics, Part B*, edited by M. N. Nabighian, pp. 521–640, Soc. of Explor. Geophys., Tusla, Okla.

Medina, F., T. González-Morán, and L. González (1990), Gravity and seismicity analyses of the El Chichón volcano, Chiapas, Mexico, *Pure Appl. Geophys.*, *133*, 149–165, doi:10.1007/BF00876708.

Milsom, J. (1996), *Field Geophysics*, 187 pp., John Wiley, Chichester, U. K.

Monteiro Santos, F. A., E. P. Almeida, M. Gomes, and A. Pina (2006), Hydrogeological investigation in Santiago Island (Cabo Verde) using magnetotellurics and VLF methods, *J. Afr. Earth Sci.*, *45*, 421–430, doi:10.1016/j.jafrearsci.2006.03.012.

Mulleried, F. K. G. (1933), El Chichón, único volcán en actividad en el sureste de México, *Rev. Inst. Geol.*, *33*, 156–170.

Napoli, R., G. Currenti, and C. Negro (2007), Internal structure of Ustica volcanic complex (Italy) based on a 3D inversion of magnetic data, *Bull. Volcanol.*, *69*, 869–879, doi:10.1007/s00445-007-0115-8.

Nixon, G. T. (1982), The relationship between Quaternary volcanism in central Mexico and the seismicity and structure of subducted ocean lithosphere, *Geol. Soc. Am. Bull.*, *93*, 514–523, doi:10.1130/0016-7606(1982)93<514:TRBQVI>2.0.CO;2.

Nooren, C. A. M., W. Z. Hoek, L. A. Tebbens, and A. L. Martin del Pozzo (2009), Tephrochronological evidence for the late Holocene eruption history of El Chichon Volcano, Mexico, *Geofis. Int.*, *48*, 97–112.

Parasnis, D. S. (1997), *Principles of Applied Geophysics*, 5th ed., 429 pp., Chapman and Hall, London.

Pirttijärvi, M. (2004), Karous-Hjelt and Fraser filtering of VLF measurements, report, Univ. of Oulu, Oulu, Finland. (Available at http://www.cc.oulu.fi/~mpi/Softat/Khffilt.html)

Rampino, M. R., and S. Self (1984), Sulphur-rich volcanic eruptions and stratospheric aerosols, *Nature*, *310*, 677–679, doi:10.1038/310677a0.

Rose, W. I., T. J. Bornhorst, S. P. Halsor, W. A. Capaul, P. S. Plumley, S. De La Cruz-Reyna, M. Mena, and R. Mota (1984), Volcan El Chichón, Mexico: Pre-1982 S-rich eruptive activity, *J. Volcanol. Geotherm. Res.*, *23*, 147–167, doi:10.1016/0377-0273(84)90060-X.

Rouwet, D., Y. A. Taran, and N. R. Varley (2004), Dynamics and mass balance of El Chichón crater lake, Mexico, *Geofis. Int.*, *43*, 427–434.

Rouwet, D., Y. Taran, S. Inguaggiato, N. Varley, and J. A. Santiago (2008), Hydrochemical dynamics of the "lake-spring" system in the crater of El Chichón volcano (Chiapas, Mexico), *J. Volcanol. Geotherm. Res.*, *178*, 237–248, doi:10.1016/j.jvolgeores.2008.06.026.

Rouwet, D., S. Bellomo, L. Brusca, S. Inguaggiato, M. Jutzeler, R. Mora, A. Mazot, R. Bernard, M. Cassidy, and Y. Taran (2009), Major and trace element geochemistry of El Chichon volcano-hydrothermal system (Chiapas, Mexico) in 2006–2007: Implications for future geochemical monitoring, *Geofis. Int.*, *48*, 55–72.

Schmincke, H.-U. (2004), *Volcanism*, 324 pp., Springer, New York.

Scolamacchia, T., J. L. Macías, M. F. Sheridan, and S. R. Hughes (2005), Morphology of ash aggregates from wet pyroclastic surges of the 1982 eruption of El Chichón Volcano, Mexico, *Bull. Volcanol.*, *68*, 171–200, doi:10.1007/s00445-005-0430-x.

Servicio Geológico Mexicano (2006), Carta magnética de campo total, Villahermosa E15–8, Tabasco, scale 1:250,000, Hidalgo, Mexico. (Available at http://portaljsp.sgm.gob.mx/cartas_impresas/productos/cartas/cartas250/geofisica/pdf/106_E15-8_GF.pdf)

Sharma, S. P., and V. C. Baranwal (2005), Delineation of groundwater-bearing fracture zones in a hard rock area integrating very low frequency electromagnetic and resistivity data, *J. Appl. Geophys.*, *57*, 155–166, doi:10.1016/j.jappgeo.2004.10.003.

Stoiber, R. E., and M. J. Carr (1973), Quaternary volcanic and tectonic segmentation of Central America, *Bull. Volcanol.*, *37*, 304–325, doi:10.1007/BF02597631.

Taran, Y. A., and L. Peiffer (2009), Hydrology, hydrochemistry and geothermal potential of El Chichón volcano-hydrothermal system, Mexico, *Geothermics*, *38*, 370–378, doi:10.1016/j.geothermics.2009.09.002.

Taran, Y. A., and D. Rouwet (2008), Estimating thermal inflow to El Chichón crater lake using the energy-budget, chemical and isotope balance approaches, *J. Volcanol. Geotherm. Res.*, *175*, 472–481, doi:10.1016/j.jvolgeores.2008.02.019.

Taran, Y. A., T. P. Fischer, B. Pokrovsky, Y. Sano, M. A. Armienta, and J. L. Macías (1998), Geochemistry of the volcano-hydrothermal system of El Chichón Volcano, Chiapas, Mexico, *Bull. Volcanol.*, *59*, 436–449, doi:10.1007/s004450050202.

Taran, Y. A., D. Rouwet, S. Inguaggiato, and A. Aiuppa (2008), Major and trace element geochemistry of neutral and acidic thermal springs at El Chichón Volcano, Mexico, *J. Volcanol. Geotherm. Res.*, *178*, 224–236, doi:10.1016/j.jvolgeores.2008.06.030.

Tassi, F., O. Vaselli, B. Capaccioni, J. L. Macías, A. Nencetti, G. Montegrossi, and G. Magro (2003), Chemical composition of fumarolic gases and spring discharges from El Chichón volcano, Mexico: Causes and implications of the changes detected over the period 1998–2000, *J. Volcanol. Geotherm. Res.*, *123*, 105–121, doi:10.1016/S0377-0273(03)00031-3.

Tassi, F., B. Capaccioni, F. Capecchiacci, and O. Vaselli (2009), Non-methane volatile organic compounds (VOCs) at El Chichon volcano (Chiapas, Mexico); geochemical features, origin and behavior, *Geofis. Int.*, *48*, 85–95.

Templos, L. A. (1981), Observaciones geoquímicas de la zona geotérmica del Chichonal, Chiapas, report, Com. Fed. de Electr., Mexico City.

Tilling, R. I. (1982), The 1982 eruption of El Chichón volcano, southeastern Mexico, *Earthq. Inf. Bull.*, *14*, 164–172.

Tilling, R. I. (2009), El Chichon's "surprise" eruption in 1982: Lessons for reducing volcano risk, *Geofis. Int.*, *48*, 3–19.

Varekamp, J. C., J. F. Luhr, and K. L. Prestegaard (1984), The 1982 eruptions of El Chichón volcano (Chiapas, Mexico): Character of the eruption, ash-fall deposits, and gas phase, *J. Volcanol. Geotherm. Res.*, *23*, 39–68, doi:10.1016/0377-0273(84)90056-8.

Zablocki, C. J. (1978), Applications of the VLF induction method for studying some volcanic processes of Kilauea volcano, Hawaii, *J. Volcanol. Geotherm. Res.*, *3*, 155–195, doi:10.1016/0377-0273(78)90008-2.

Zlotnicki, J., G. Vargemezis, A. Mille, F. Bruère, and G. Hammouya (2006), State of the hydrothermal activity of Soufrière of Guadeloupe volcano inferred by VLF surveys, *J. Appl. Geophys.*, *58*, 265–279, doi:10.1016/j.jappgeo.2005.05.004.

Zlotnicki, J., et al. (2009), Combined electromagnetic, geochemical and thermal surveys of Taal volcano (Philippines) during the period 2005–2006, *Bull. Volcanol.*, *71*, 29–47, doi:10.1007/s00445-008-0205-2.

M. Jutzeler and M. Roach, Centre of Excellence in Ore Deposits, University of Tasmania, Private Bag 79, Hobart, TAS 7001, Australia. (jutzeler@gmail.com)

N. Varley, Facultad de Ciencias, Universidad de Colima, Bernal Díaz del Castillo #340 Col. Villas San Sebastián, C.P. 28045, Colima, Mexico.